Characterization of UHF Radio Propagation Channels in Tunnel Environments for Microcellular and Personal Communications

Y. P. Zhang and Y. Hwang

***Abstract*— Narrowband and wideband propagation measurements have been conducted in five tunnels. The effects of pedestrians, vehicles, and curvature on propagation are included in the characterization. The narrowband propagation is characterized in terms of power distance law, slow fading, and fast fading statistics: wideband propagation, rms delay spread, and its statistics. The results show that the power distance law is insensitive to the location of the transmit antenna in the cross section of a tunnel, but not to the antenna insertion loss. The lognormal distribution basically fits the slow variation of the received signals, whereas the Rician distribution, the fast fading in the straight empty sections of the tunnels. In the curved tunnel sections, the Rayleigh distribution does not fit the fast fading variation as is expected. Tunnel radio propagation channels are dependent strongly upon frequency. Higher frequency signals exhibit more severe fluctuations and larger rms delay spread. The rms delay spreads are found to be generally less than 25 and 103 ns for the emptied and occupied tunnel conditions, respectively. One can conclude that the tunnel channels have a broad coherent bandwidth and can support the data rate up to 1 Mb per second without equalization.**

***Index Terms*— Personal communications, underground microcellular, underground radio propagation channels.**

I. Introduction

EXTENSIVE studies have been undertaken to understand both narrow and wideband UHF radio propagation channels in various environments for mobile and personal communications [1]. UHF radio wave propagation in rural areas has been reported in [2]–[4]. Research on UHF radio channels in suburban areas have been performed by several researchers [5], [6]. UHF propagation characteristics in urban areas have received much greater attention since the vast majority of mobile communication systems operate in the centers of population [7]–[15]. As wireless communications is permeating personal communications across the world, propagation research has concentrated on the characterization of UHF radio channels in indoor environments such as houses, office buildings, and factories [16]–[27]. Regardless of the type of communications environment, received a signal consists of reflected and diffracted waves in addition to the direct wave. The multipath propagation channels result in signal fluctuations and intersymbol interference. Due to the undeterministic nature of the signal structure, radio propagation channels generally have been characterized statistically.

Tunnels exist in metropolitan cities and mountainous areas. Radio coverage is needed for personal and emergency communications. As a result, a few investigations into tunnel UHF radio propagation channels have been carried out [28]–[35]. Previous experimental studies of radio wave propagation characteristics in tunnel environments were almost entirely concentrated on finding the optimum frequency bands for minimum attenuation. The results showed that the optimum frequency window seems to be between 1–2 GHz. The propagation attenuation in the far region of a straight tunnel is less than that in free space, thus indicating that guided-wave phenomena are involved. The confined spaces of tunnels have been modeled as oversized imperfect waveguides. The received field is the sum of the fields consisting of a fundamental mode and an infinite number of higher order modes. The higher order modes caused by the imperfections of the tunnel structure have also been found to play an important role in propagation. Similar to multipath propagation, multimode propagation has produced signal fluctuations and intersymbol interference. As these propagation modes are converted in an undetermined nature, tunnel UHF radio channels should also be characterized statistically. To date, even the knowledge of the deterministic characteristics of narrowband tunnel UHF radio propagation channels is very limited. It is the objective of this study to provide the propagation characteristics of both narrow and wideband radio propagation channels in tunnel environments at 900 and 1800 MHz.

Measurements have been conducted in the tunnels of the People's Republic of China and Hong Kong. Analysis of narrowband experimental data reveals that power distance factors range from 1.87 to 4.49 with a standard deviation of 3.69–7.37. The effects of pedestrians, vehicles, and curvature cause extra losses from 6 to 30 dB. The slow variations of the received signals follow the lognormal distribution with averaged standard deviations of 4.7 dB for a 900-MHz channel. The fast fading component distributions about the local median in the straight sections of the tunnels follow closely to Rician distribution with $4 < K < 8$ dB, where K is the ratio of the dominant mode signal to higher order mode signals. In the curved sections, the fast fading distributions do not fit the Rayleigh distribution as well as expected. The experimental data also indicate a broad coherence bandwidth characteristic of the tunnel radio propagation channel. The rms

Manuscript received February 28, 1995; revised September 30, 1996. This work was supported by the National Natural Science Foundation of China.

The authors are with the Department of Electronic Engineering, City University of Hong Kong.

Publisher Item Identifier S 0018-9545(98)00110-8.

delay spread shows a clear dependence on frequency. Higher frequency causes a larger rms delay spread. The rms delay spread is found to be less than 25 and 103 ns for the emptied and occupied tunnel conditions, respectively. Thus, data rate up to one megabit per second without equalization can be supported in tunnel environments.

Section II attempts to review the deterministic characteristics of tunnel UHF radio propagation and defines the parameters quantifying the characteristics of narrow and wideband tunnel UHF radio propagation channels and their statistics. Section III describes the experimental setups, tested tunnel environments, and testing procedures. Section IV analyzes the measured data, and Section V summarizes the conclusions.

II. Background

A. Deterministic Tunnel Propagation Characteristics

This section briefly reviews the deterministic radio wave propagation characteristics in empty, straight, and unobstructed tunnels. The cross section of tunnels is usually rectangular or arched shaped. Let us consider a rectangular tunnel as an example, for the conclusions for arched-shaped tunnels will be very similar. The deterministic radio wave propagation characteristics are obtained experimentally. A rectangular tunnel is modeled as an oversized imperfect rectangular waveguide. According to the theory, the radio wave propagation in tunnel environments should exhibit the cutoff phenomena, that is, only those signals with frequencies higher than the so-called tunnel cutoff frequency can propagate. The cutoff frequency for a rectangular tunnel can be roughly estimated as [33]

$$f_c = \frac{1}{2\sqrt{\mu_0\varepsilon_0}}\sqrt{\left(\frac{m}{A}\right)^2+\left(\frac{n}{B}\right)^2} \quad \text{(Hz)} \tag{1}$$

where A and B represent the tunnel width and height, respectively. For most tunnels, the cutoff frequency is about tens of megahertz. The radio wave propagation frequencies allocated to current cellular mobile and personal communications are above the cutoff frequency, and, therefore, the propagation involves many hybrid electromagnetic modes HEM_{mn} of which HEM_{11} mode is a fundamental one. Their propagation constants [33] can be expressed, provided $m\lambda \ll 4A$ and $n\lambda \ll 4B$ as

$$\begin{aligned}\gamma = \alpha + j\beta \approx{}& \frac{1}{A}\left(\frac{m\lambda}{4A}\right)^2 \text{Re}\left(\frac{\left(\frac{\varepsilon_a^*}{\varepsilon_0}\right)}{\sqrt{\left(\frac{\varepsilon_a^*}{\varepsilon_0}\right)-1}}\right) \\ &+ \frac{1}{B}\left(\frac{n\lambda}{4B}\right)^2 \text{Re}\left(\frac{1}{\sqrt{\left(\frac{\varepsilon_a^*}{\varepsilon_0}\right)-1}}\right) \\ &+ j\frac{2\pi}{\lambda}\left(1-\frac{1}{2}\left(\frac{m\lambda}{4A}\right)^2-\frac{1}{2}\left(\frac{n\lambda}{4B}\right)^2\right)\end{aligned} \tag{2}$$

where λ is the wavelength and "Re" means the real part of the variable. The real part of (2) indicates that the attenuation of the radio wave propagation in an empty, straight, and unobstructed rectangular tunnel is proportional directly to the square of wavelength and inversely to the cubes of the transverse dimensions A and B. The imaginary part of (2) reflects the phase difference of different HEM_{mn} modes with respect to propagation in free space. The higher the mode order, the larger the attenuation and the phase difference will be. These multimodes will result in signal fluctuations and intersymbol interference. Furthermore, all actual tunnels deviate from a perfect theoretical model. They are not always straight and empty, but may be curved, branched, or with obstacles inside. These realistic environments will cause additional mode conversion and increase signal attenuation. This type of mode conversion will make the number of propagating electromagnetic modes excited in an undeterministic way. Consequently, signal fluctuations and intersymbol interference in tunnel environments will behave in a random manner. Statistical characterization will clearly represent the propagation behavior from practical and system points of view.

B. Parameters to Characterize Narrowband Radio Propagation Channels

Signal fluctuations can be decomposed into slow fading engendered by the global mode variations and fast fading caused by the interference of local modes. Slow and fast fading for many mobile and personal radio environments have been found to follow theoretical lognormal distributions, Rician or Rayleigh, respectively. As the propagation in tunnel environment can be described by the fundamental mode and higher order modes, we conjecture that these two distributions can also be applied to tunnel radio propagation as well.

The lognormal probability density in decibel values is described by a Gaussian distribution of the mean η and of the standard deviation δ

$$P(r) = \frac{1}{\delta\sqrt{2\pi}}\exp\left(-\frac{(r-\eta)^2}{2\delta^2}\right). \tag{3}$$

The Rice probability density in decibel terms is given by [1]

$$\begin{aligned}P(r) = \frac{1}{8.68\alpha^2}\exp\left(\frac{r}{4.34}-\frac{(d^2+\exp(r/4.34))}{2\alpha^2}\right) \\ \times I_0\left(\frac{d}{\alpha^2}\exp\left(\frac{r}{4.34}\right)\right)\end{aligned} \tag{4}$$

where $I_0(x)$ is a modified Bessel function of order zero and d is the dominant mode signal. This dominant mode signal can decrease the standard deviation of the received signal envelope if it increases relative to higher order mode signals. The $d=0$ in (4) yields the Rayleigh probability density. The mean of the Rice probability density is expressed as [36], [37]

$$\eta = \exp(-y)\alpha\sqrt{\frac{\pi}{2}}[(1+2y)I_0(y)+2yI_1(y)] \tag{5}$$

where $I_1(y)$ is a modified Bessel function of order 1 and $y = d^2/4\alpha^2$. The standard deviation is expressed as [36]

$$\delta = \sqrt{d^2+2\alpha^2-1}. \tag{6}$$

In (5) and (6), η and δ are obtained after the researchers have statistically analyzed the experimental data files. Hence, simultaneous solution to (5) and (6) will find the parameters α

and d of the theoretical Rice probability density. The impact of the conversion of higher order modes to the dominant mode signal can be described by the ratio of the dominant mode signal to higher order mode signals as

$$K = 10\log(d^2/2\alpha^2). \tag{7}$$

In addition, another key parameter to describe slow fading is power loss, which is generally represented by Z^n. Z is the separation between the transmit and receive antennas, and n is the power distance factor to be determined experimentally.

C. Parameters to Characterize Wideband Radio Propagation Channels

The characteristics of wideband radio propagation channels can be roughly quantified by the mean excess delay τ_m and root-mean-square delay spread $\tau_{\rm rms}$ defined as

$$h_a(\tau) = \int_p h_c(p,\tau)\,dp \tag{8}$$

where the impulse response $h_c(p,\tau)$ is actually a power delay profile obtained from measurements and scaled such that the first wave arrives at $\tau = 0$ in a profile and $h_a(\tau)$ is the space-averaged power delay profile and is given by

$$h_{na}(\tau) = \frac{h_a(\tau)}{\int_0^\infty h_a(\tau)\,d\tau} \approx \frac{h_a(\tau)}{\sum_k h_a(\tau_k)} \tag{9}$$

where $h_{na}(\tau)$ is normalized $h_a(\tau)$

$$\tau_m = \int_0^\infty \tau h_{na}(\tau)\,d\tau \approx \frac{\sum_k \tau_k h_a(\tau_k)}{\sum_k h_a(\tau_k)} \tag{10}$$

where τ_m is the first moment of the power delay profile with respect to the first arriving mode. The delay spread $\tau_{\rm rms}$ is the square root of the second central moment of the power delay profile and expressed as

$$\begin{aligned}\tau_{\rm rms} &= \left[\int_0^\infty (\tau-\bar{\tau})^2 h_{na}(\tau)\,d\tau\right]^{1/2} \\ &\approx \left[\frac{\sum_k \tau_k^2 h_a(\tau_k)}{\sum_k h_a(\tau_k)} - (\bar{\tau})^2\right]^{1/2}\end{aligned} \tag{11}$$

where $\tau_{\rm rms}$ gives an indication of the potential for the intersymbol interference.

III. Experiments

The experimental setups and techniques are presented in this section. Five tunnels, a representation of tunnels having both straight and curved sections, were used in our measurements, with the first four located in the People's Republic of China: 1) the Taiyuan Fen Hou (TFH) tunnel; 2) Taiyuan Coal Mine Haulageway (TCMH) tunnel complex; 3) Shanxi Institute of Mining and Technology (SIMT) tunnel; 4) Taiyuan Underground Market (TUM) tunnel; and 5) Hong Kong (NS 173) tunnel. Each tunnel under test is described in the Appendix.

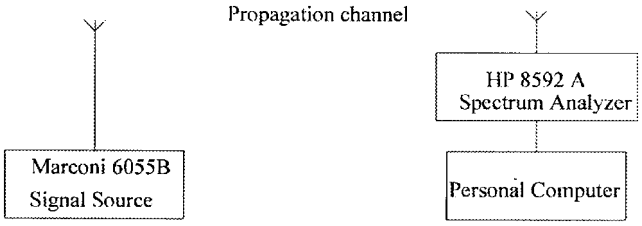

Fig. 1. The narrowband experiment setup.

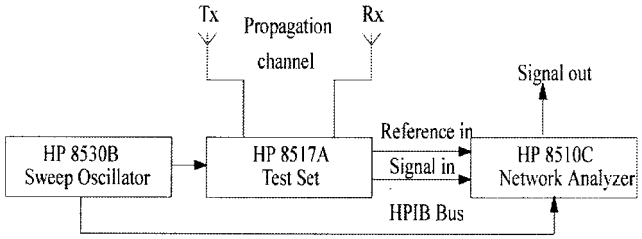

Fig. 2. The wideband experiment setup.

A. Experimental Setups

The narrowband experiment setup is shown in Fig. 1. It consists of three modules: 1) a Marconi 6055B signal source used as the transmitter; 2) an HP 8592A spectrum analyzer used as the receiver; and 3) a personal computer used as the data collector for subsequent analysis. This narrowband experiment system was calibrated with 120-dB dynamic range.

The wideband experiment setup is shown in Fig. 2. The system consists of an HP 8350B sweep oscillator, 8510C network analyzer, and 8517A S-parameter test set. Port 1 was connected to the transmit antenna through a 10-m coaxial cable. The power outputted to the transmit antenna was 15 dBm. The transmitted sweep frequency waves were captured by the receive antenna connected to port 2 through another 50-m cable. The measured data of wideband propagation characteristics was stored onto a floppy disk of the network analyzer for subsequent analysis.

In probing the tunnel narrowband propagation characteristics, a standard half-wave dipole was employed. For the tunnel wideband propagation channel measurements, the discone antenna designed for broad bandwidth was used.

B. Experimental Techniques

Prior to describing the experimental procedures, the coordinate system of a typical tunnel complex is defined for reference in the subsequent data analysis. Z axis is defined as the longitudinal direction of the main tunnel, X axis as the width, and Y axis as the height. The width and height of the main tunnel are described by A and B, respectively. As for the branch tunnels, their boundaries can be easily determined with respect to the main tunnel. The antennas under test are specified in terms of both location and polarization. For example, if both the transmit and the receive antennas are parallel to the floor and perpendicular to the sidewalls, they are referred by (HI-HI) with "H" standing for horizontal orientation and "I" the middle position. The first one in the bracket represents the transmit antenna, and the second one

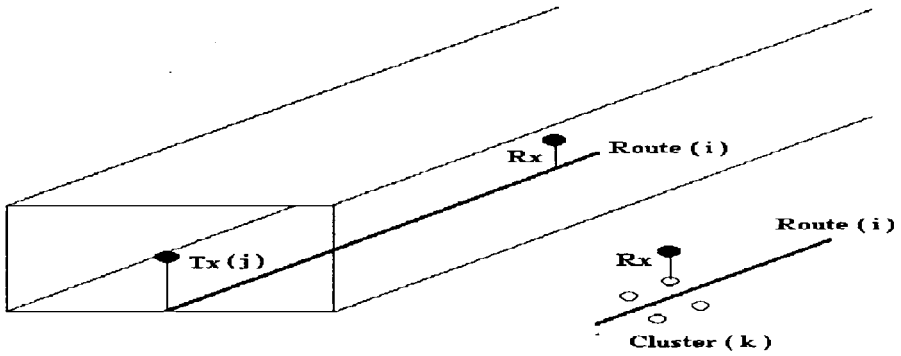

Fig. 3. The experiment pattern showing the transmit and receive antenna positions.

represents the receive antenna. The position is further clarified by (X, Y, Z). In the above arrangement, they are denoted by $(0.5A, 0.5B, Zo)$ and $(0.5A, 0.5B, Z)$, respectively, where Zo is used as reference. The experimental data files were compiled based on the tunnel, transmitter output power, antenna arrangement, frequency, blockage, and narrow/widebands.

The technique of the narrowband propagation measurements is similar to that suggested in [1]. Fig. 3 depicts the experimental pattern of the tunnel special radio environments and probed tunnel narrowband channels. Three transmit antenna positions and five receive antenna routes were selected. We first fixed the transmit antenna in position one $(0.5A, 0.5B, Zo)$ with different positions of the receive antenna connected with the receiver and the data-acquisition modules of the narrowband system. The whole receive unit was housed on a trolley moving along the first three selected routes $(0.2A, 0, Z)$, $(0.5A, 0, Z)$, and $(0.8A, 0, Z)$ to sound the tunnel narrowband channels in the longitudinal direction. We also measured the fluctuations of received signals in transverse direction along the last two routes: $(0.5A, Y, Z1)$ and $(X, 0.5B, Z1)$. The process was repeated until all antenna arrangements were exhausted. The spatial sampling distances were set to 3 and 1 cm at frequencies of of 900 and 1800 MHz, respectively. Such sampling distances were sufficient to follow the fast fading component of a received signal. The sampling pulses were generated by a tachogenerator attached to the fifth wheel of the trolley. Most experimental studies of tunnel propagation characteristics adopted a sampling distance that was usually longer than signal wavelength, thus resulting in a loss of the fast fading components of received signals.

Wideband propagation measurements were performed using the swept frequency technique [21]. In this technique, the channel was excited at central frequencies of 900 and 1800 MHz with frequency components over a 400-MHz band. The distorted version of each frequency component caused by the tunnel environments was measured. The inverse FFT of the measured frequency domain data was taken to provide the wideband characteristics of tunnel propagation channels. The tunnel wideband propagation channels were measured in a similar manner as illustrated in Fig. 3 on a cluster scale, with the cluster having a size of 16 cm^2. The adjacent cluster on the route was 1 m apart for most measurements. Four individual impulse responses, $h_c(p, \tau)$ were obtained for each cluster. Each individual impulse response was measured over several hundred microseconds. They were then averaged at each time delay to calculate an averaged impulse response $h_a(\tau)$ to simulate a time-invariant condition. This averaged impulse response was computed to characterize the wideband characteristics of tunnel propagation channels.

IV. Results and Discussion

A. Tunnel UHF Narrowband Radio Propagation Characteristics

A typical randomly selected received signal segment of horizontal polarization at 900 MHz along route (2) of the straight section of the TCMH tunnel is shown in Fig. 4(a). Another typical randomly selected received 1800-MHz signal segment of horizontal polarization in the curved section of the NS 173 tunnel is illustrated in Fig. 4(b). As expected, the received signal drops dramatically and exhibits more variability as the receiving antenna is not in the line-of-sight region. Fig. 5(a) and (b) shows the received signals at the frequency of 900 MHz for horizontal polarization along measurement paths (5) and (4) in both main and branch sections of the TCMH tunnel. It can be seen that the longitudinal pattern of the received signal decreases with the increasing separation between the transmit and receive antennas. The transversal pattern of the received signal shows a distorted dominant-mode cosine function.

1) Power Distance Law: The power distance dependence is a multivariable function of tunnel geometry, electromagnetic parameters, such as frequency, antenna position, polarization, and imperfections of the tunnels, and the environment. Fig. 6 is a plot of the averaged relative power received by moving the receiver along the middle of the SIMT main tunnel in the longitudinal direction with three transmit antenna positions at the frequency of 900 MHz for vertical polarization. Curves (1), (2), and (3) in Fig. 6 represent the power distance variation for three different positions of the transmit antenna: middle, upper middle, and upper-left corner of the tunnel cross section. The attenuation is almost the same for three cases, but with different transmit antenna insertion power loss. One can conclude that for the dipole antenna, the received signal has 10-dB differential for each different location. Similar results were observed for the horizontal polarization, 1800-MHz frequency, and other tunnels. The dipole antenna is

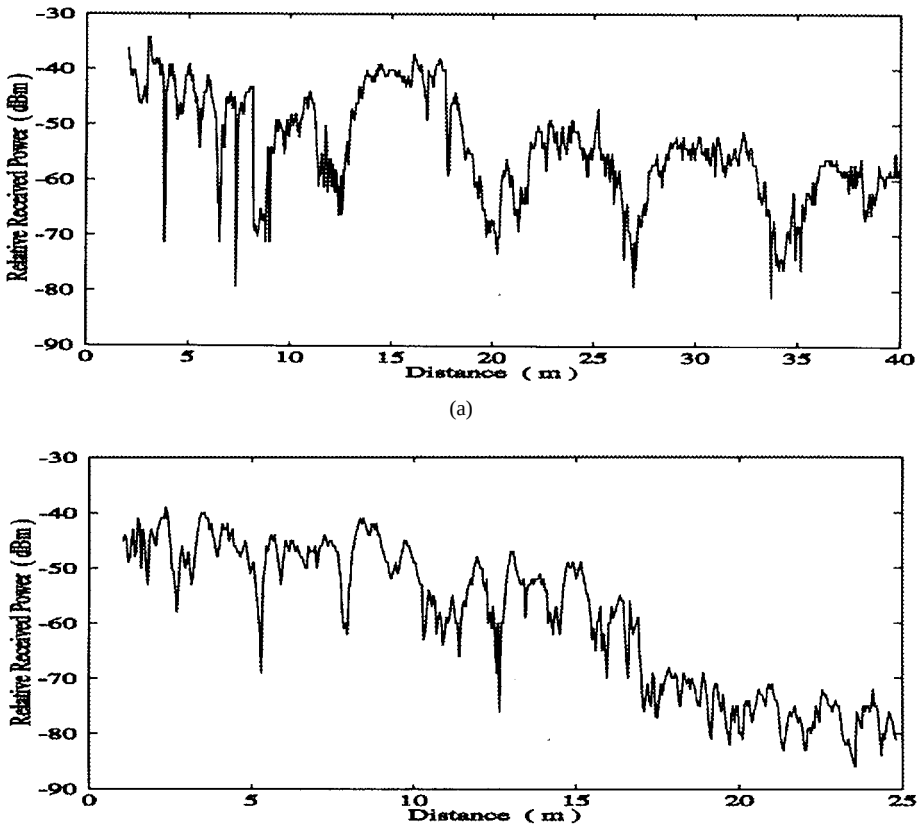

Fig. 4. (a) Signal segment received along the longitudinal direction of the straight section of the TCMH tunnel. (b) Signal segment received along the longitudinal direction of the curved section of the NS 173 tunnel.

generally designed and used for open space communications. As a result, it is matched to free space, but not to tunnel-confined spaces. This can be verified by the fact that when the antenna is located in the middle of the tunnel, the insertion loss is minimum. The middle position is closer to a free-space environment than the other two positions. Once the energy is radiated, the attenuation is mostly governed by the propagation characteristics of the tunnel.

The power distance factor was determined in the conventional manner by applying regression analysis to the slow fading component of a received signal data file. A linear fit was made to the local mean of the received signal in decibels versus distance from transmitter to receiver on a logarithmic scale. The gradient of the fitted line gives the power distance factor. Table I shows the power distance factors and the standard deviations obtained according to the criteria of the least mean square for straight and unobstructed sections of the five tunnels. It is found that horizontally polarized signals have smaller power distance factors than vertically polarized ones due to the smaller attenuation constant for the former than the latter. In addition, comparison with the power distance factors in the NS 173 tunnel at frequencies of 900 and 1800 MHz reveals that higher frequency signal has a smaller power distance factor. This is contrary to what has been found in other radio propagation environments. Note our measured power distance factors are also different from that predicted by tunnel imperfect waveguide theory. The power distance factor was determined to be one [28] in which only the fundamental mode was considered. Experimental data observed that the contribution of the signal was from not only the fundamental mode, but also other significant higher order ones. This discrepancy of the previous imperfect waveguide theory was rectified somewhat by including other loss mechanisms such as the mode conversion due to either tilts or roughness of tunnel walls.

TABLE I

Tunnel	No. of files		900 MHz			
	HP	VP	n_v	SD v dB	n_h	SD h dB
TFH	9	9	4.44	7.37	3.87	5.50
TUM	9	9	3.71	4.97	2.96	5.42
SIMT	9	9	2.49	5.21	2.21	4.47
TCMH	9	9	2.37	3.69	1.87	7.32
NS173	9	9	4.49	5.04	4.20	5.01
NS173	9	9	1800 MHz			
			2.46	6.34	2.12	6.07

The effects of pedestrians and vehicles in tunnel environments were also investigated. One will expect that the existence of obstruction, whether they are pedestrians or vehicles, causes blockage and additional mode conversion and thus increases the propagation loss. Measurements in the TUM

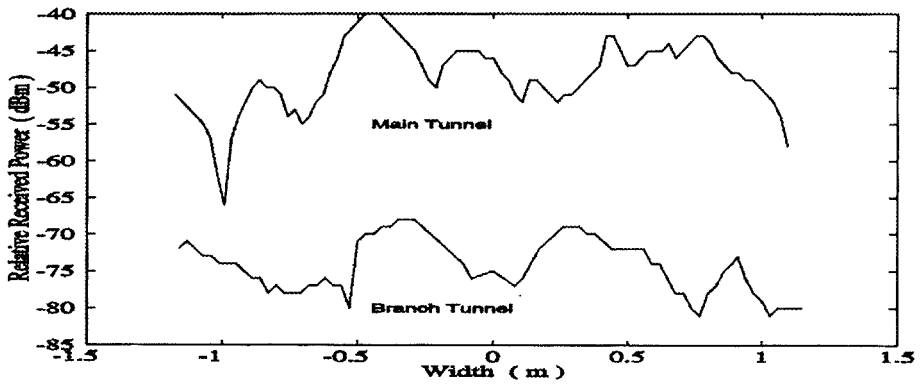

(a)

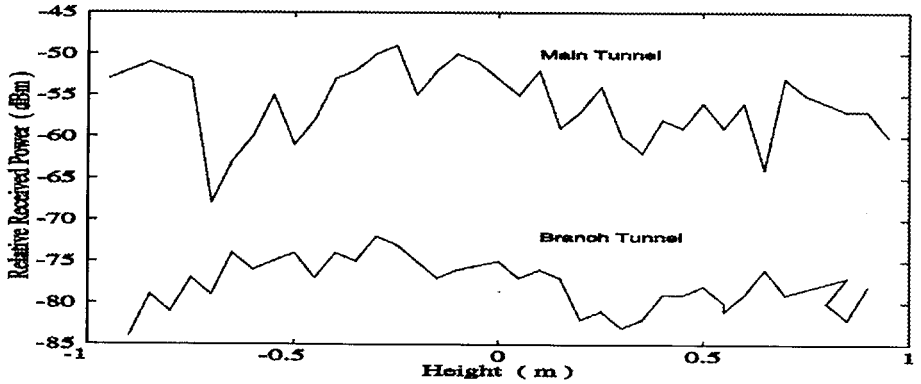

(b)

Fig. 5. (a) Received signals versus width of both the TCMH main tunnel and its branch one. (b) Received signals versus height of both the TCMH main tunnel and its branch one.

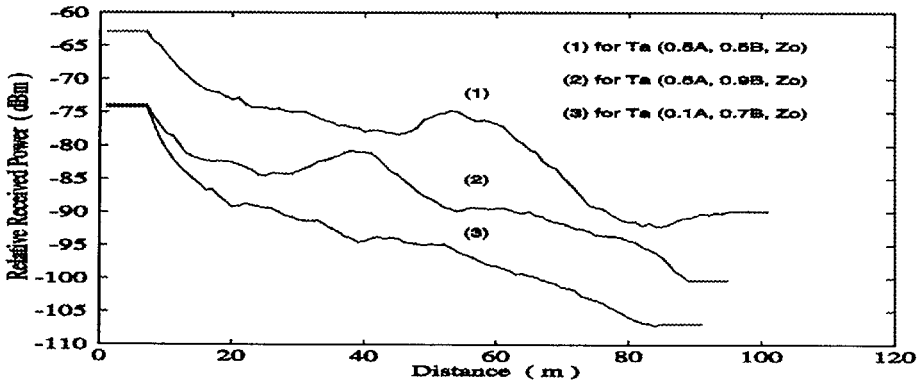

Fig. 6. Plot of power distance dependence on the transmit antenna positions in the straight section of the SIMT tunnel.

tunnel were taken in daytime over different time periods to account for the variation in pedestrian density. The power distance factors at the frequency of 900 MHz for horizontally and vertically polarized signals showed an increase from 2.96 to 3.71 for the almost emptied tunnel to 3.17–5.49 for fully occupied tunnel conditions. The measurements in the TCMH tunnel indicated a 13-dB shadowing loss at the frequency of 900 MHz caused by the coal mine train. The shadowing loss due to a car or a truck was measured in the TFH tunnel. The truck caused 6–10-dB additional loss while the car shadowing effects were negligible.

Tunnel curvature should yield more shadowing loss for the received signals in the out-of-sight region. Curvature extra loss around the junctions of the TCMH tunnel was measured by placing the transmitter in the middle of the branch tunnel and moving the receive antenna at half-tunnel height along route (2). An extra loss of 17 and 30 dB at 900 MHz was measured toward both the end at an abtuse angle and entry at an acute angle of the main tunnel, respectively. The investigation of the curvature extra loss dependence on frequency was conducted in the NS 173 tunnel. As expected, higher frequency caused more curvature extra loss due to the existence of a sharper penumbra region from the lit region to the shadow region. There was 9 dB more curvature extra loss at 1800 MHz with respect to 900 MHz in the NS 173 tunnel. Measurements of different polarized signals indicated that curvature loss was

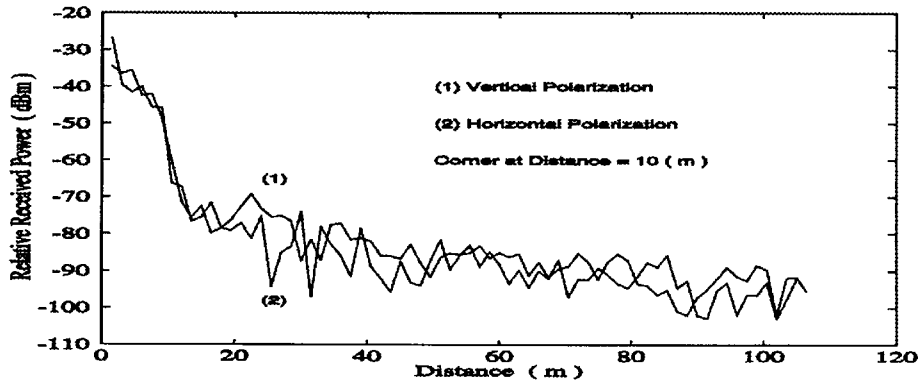

Fig. 7. A typical received signal with a corner involved along the propagation path.

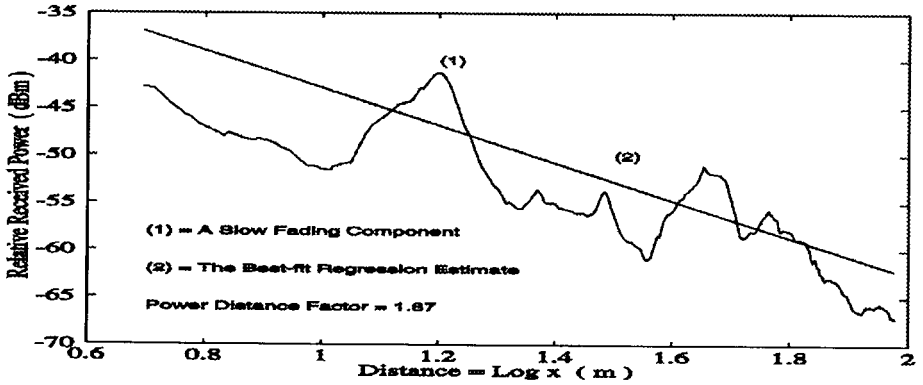

Fig. 8. Received signal slow fading component with the best-fit regression estimate.

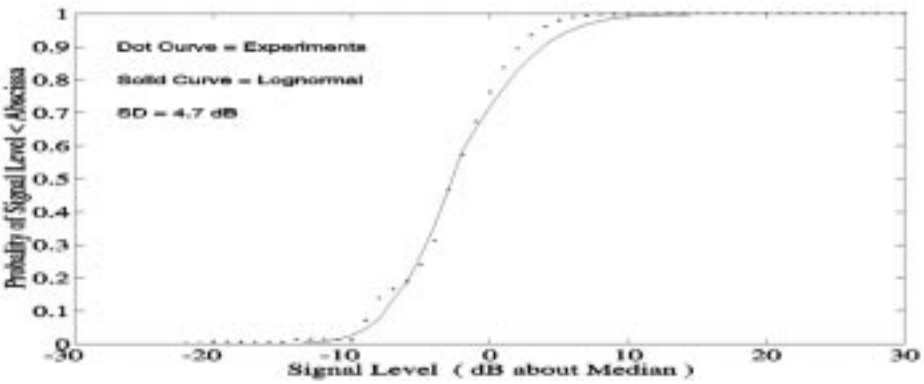

Fig. 9. Slow fading cumulative distributions of received signals in tunnel environments.

independent of polarization. The result is consistent with the theory of geometrical optics, which states that the loss due to shadowing effect is, in general, 6 dB regardless of polarization of the incident field. Fig. 7 illustrates this point where the corner was 10 m away from the transmitter. Analysis of the measured data yields the power distance factors of 3.15 and 3.09 for the 900-MHz horizontally and vertically polarized signals, respectively.

2) Slow Fading Statistics: Fig. 8 is an example of the slow fading component of a received 900-MHz signal of horizontal polarization in the TCMH tunnel together with the best-fit regression estimate. The slow fading statistics deals with the remaining variation after removal of the power distance dependence depicted by the best-fit regression estimate from each individual local mean value of the received signal power. This is useful in estimating the coverage and cochannel interference. Many other radio propagation environments predicted that slow fading would follow the lognormal probability distribution as expressed in (7). However, our measured data shows a consistent deviation from the lognormal probability distribution as presented in Fig. 9. The standard deviation is 4.7 dB. This deviation becomes worse when the signal level is moved further away from its median value. It indicates that the dominant mode and higher order modes are closely

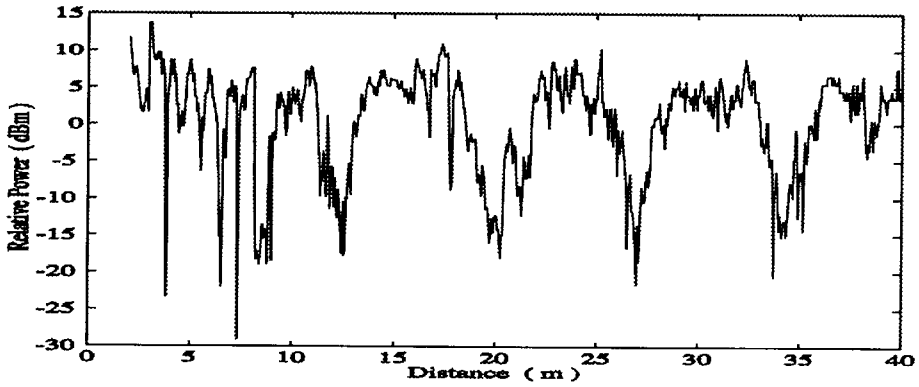

Fig. 10. Received signal fast fading component.

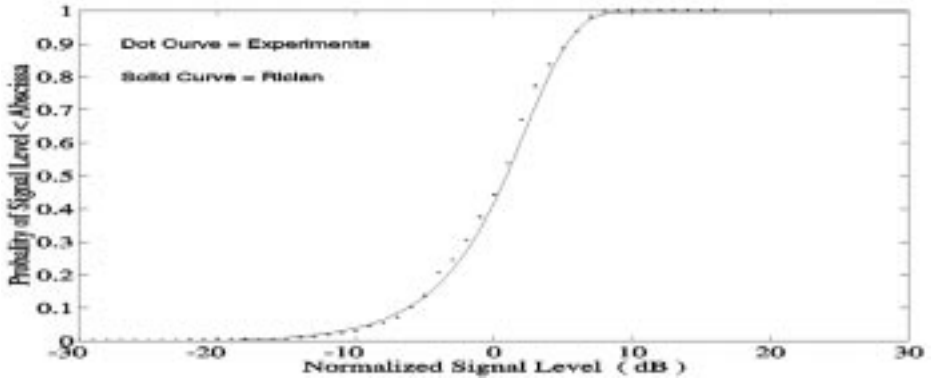

(a)

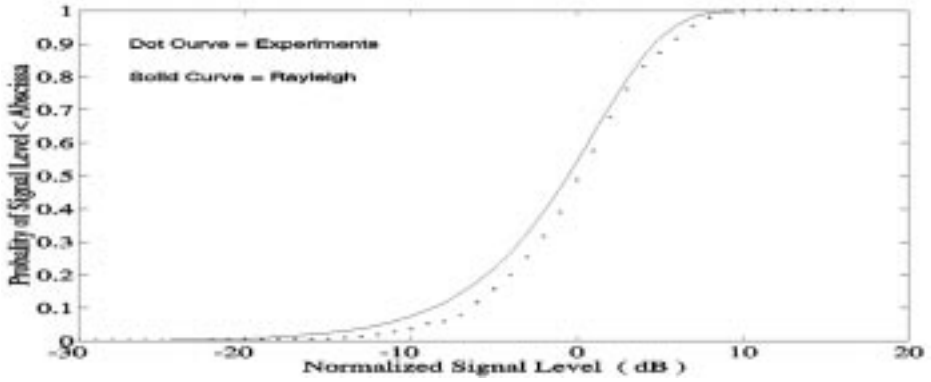

(b)

Fig. 11. Fast fading cumulative distributions of received signals in tunnel environments. (a) For straight sections. (b) For curved sections.

associated in an enclosed space of tunnel and are not randomly independent as in other radio propagation environments.

3) Fast Fading Statistics: Fast fading deteriorates the performance of a mobile radio communication system since rapid fluctuations in signal level at the moving receive antenna. As can be seen from Fig. 10, our measurements indicate that fast fading occurs in all regions. However, within the short distance region, where the receive antenna is near the transmit one, the received signal consistently shows more rapid and deeper fluctuations. A maximum fade depth of 30 dB is observed, and fade maxima is less sharper than minima. Fast fading is strongly related to the tunnel dimensions and the frequency. Fast and deep fading covers a longer distance for either the case of larger dimensional tunnel or higher frequency. These results can be explained as follows. In the short distance region, there are more significant higher order modes that cause large fluctuations, whereas in the long-distance region, as the higher order modes become less significant, only the fundamental mode, the direct incident signal, contributes the most to the received signal. Therefore, fast fading diminishes as the receiver is moving further away from the transmitter. Higher frequencies and larger dimensions will generate more significant higher order modes. As a result, the fading region will extend further. The variability of the received signals was found to be independent of horizontal and vertical polarization in the SIMT tunnel, but not in the

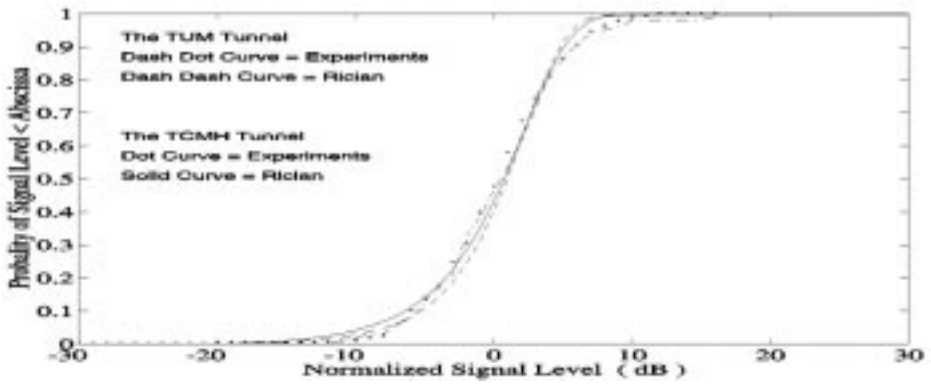

(a)

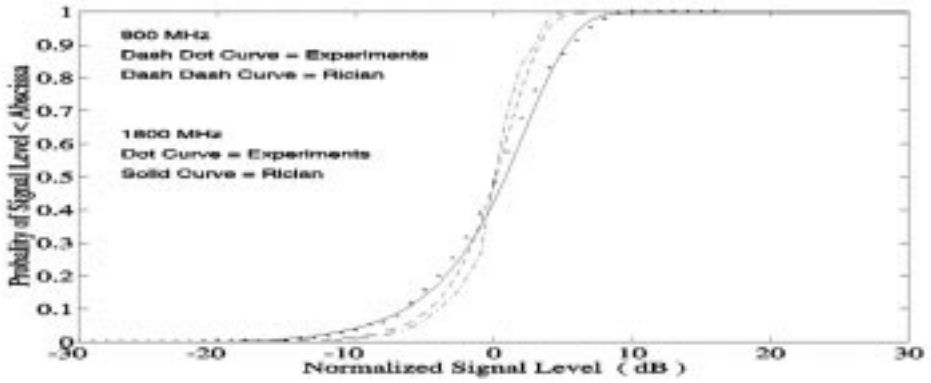

(b)

Fig. 12. Fast fading cumulative distributions of received signals. (a) For two different transversal dimensional tunnels at 900 MHz. (b) At two frequencies in the NS 173 tunnel.

TUM tunnel. The insensitivity of the received signal variability to horizontal and vertical polarization in the SIMT tunnel is likely due to its approximate square cross section, which has been further proved by the sensitivity of the received signal variability to horizontal and vertical polarization in the TUM tunnel, where the cross section is rectangular.

The fast fading component distributions about the local median were obtained for all data files and compared to theoretical Rayleigh and Rician distributions. The experimental data indicate that the fast fading of the received signal in the straight sections of a tunnel is correlated well to Rician distribution while the fast fading in the curved sections does not closely fit Rayleigh distribution as shown in Fig. 11(a) and (b). The fast fading component distributions at the frequency of 900 MHz for two different transversal dimensional tunnels were extracted and are illustrated in Fig. 12(a). The fast fading is more severe in the TUM tunnel than that of the TCMH tunnel due to the larger size of the TUM tunnel. The fast fading component distributions in the NS 173 tunnel for the frequencies of 900 and 1800 MHz were also extracted and are shown in Fig. 12(b). The higher frequency received signal exhibits more severe fluctuations due to more higher order modes generated as explained previously. Therefore, the existing conclusions on the statistical characteristics on urban, indoor, and factory UHF radio propagation channels should not be applied directly to that on the tunnel UHF radio propagation channels.

B. Tunnel UHF Wideband Radio Propagation Characteristics

1) RMS Delay Spread: To analyze measured wideband received impulse responses, one has to give careful consideration to the measurement system and the threshold level. Rappaport has developed an empirical/analytical technique to interpret the measured impulse response data [11]. In this technique, the importance of using the measurement system with sensitivity comparable to commercial radiophones was emphasized. The noise floor of -104 dBm for this 4-MHz bandwidth measurement system corresponded to the noise floor of -125 dBm for commercial 30-kHz bandwidth cellular telephones. Thus, for our 400-MHz bandwidth measurement system, the corresponding noise floor should be -84 dBm, which would yield a threshold of -74 dBm for an input SNR of 10 dB. Our threshold is between -74 and -80 dBm.

Fig. 13(a) and (b) shows the averaged 900-MHz impulse responses measured in the NS 173 tunnel with 50-m antenna separation for horizontal and vertical polarization, respectively. The arriving time of the direct wave with the largest amplitude is shown at 167 ns. The time-of-arrival of the direct wave is estimated from the length of the shortest propagation path. Before the time of 167 ns, it is noted that relative received power fluctuates below -76 dBm, which further validates our threshold level. More significant echoes for horizontal polarization than those for vertical polarization are observed. Since the attenuation for the horizontally polarized wave is

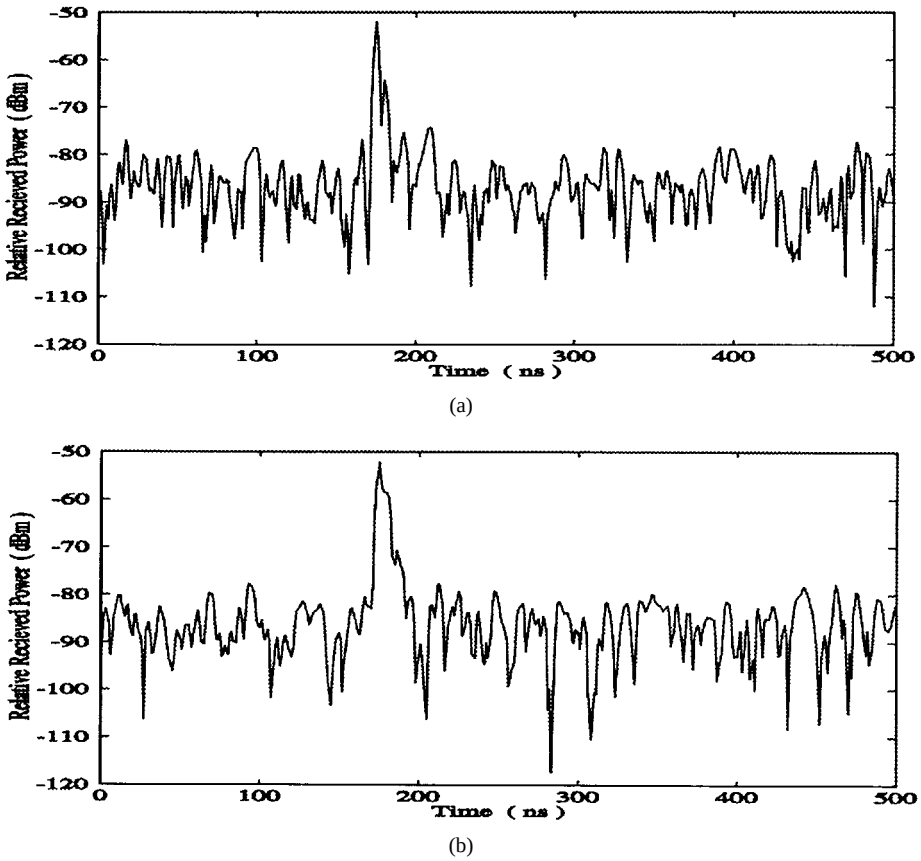

Fig. 13. (a) Averaged horizontally polarized impulse response measured in the NS 173 tunnel at the frequency of 900 MHz for line-of-sight propagation path. (b) Averaged vertically polarized impulse response measured in the NS 173 tunnel at the frequency of 900 MHz for line-of-sight propagation path.

smaller than that of the vertically polarized wave. The rms delay spread is 13.48 ns for horizontal polarization under the threshold of −76 dBm, compared with 5.49 ns for the vertical one with a threshold of −77 dBm.

Fig. 14(a) illustrates an averaged vertically polarized impulse response measured at the frequency of 1800 MHz with antenna separation of 5 m. There are two significant delayed waves. The first one, 10 dB below the direct wave, is at 36 ns. The second one, 20 dB down from the direct wave, is at 47 ns. The rms delay spread is 8.3 ns under the threshold of −80 dBm. Fig. 14(b) shows an averaged vertically polarized impulse response at the frequency of 900 MHz measured with the transmitter outside and the receiver inside the tunnel. A well-defined incident pulse is recovered because it is in the line-of-sight path. It is more interesting to note that the pulse amplitude is smaller, which indicates the difficulty of propagation from land into tunnel. The delayed waves have longer time span with 36.90 ns of rms delay spread under the threshold of −75 dBm.

Fig. 15(a) and (b) shows measurements made for the tunnel with a model vehicle. Fig. 15(a) shows the case where the antenna separation was 20 m with the vehicle located at the middle. The direct wave arrives at 67 ns. Several delayed waves with larger amplitude than the direct wave are also shown. The rms delay spread is 76.23 ns under the threshold of −75 dBm. The impulse response was recorded again when the vehicle was relocated at 40 m from the transmit antenna. The direct wave now in the line-of-sight path is recovered to maximum field intensity at 67 ns. The delayed wave at 200 ns is due to the reflection from the vehicle. The change of the arriving time of this delayed wave correlates to the change of the distance between the receive antenna and vehicle. Longer distance results in greater rms delay spread. For the impulse response shown in Fig. 15(b), the rms delay spread with the threshold of −75 dBm is 96.86 ns, which shows more spreading than an obstructed line-of-sight propagation path.

One can conclude that rms delay spreads are generally less than 25 ns for the straight empty tunnel and increases to 103 ns for the tunnel occupied by vehicle.

2) RMS Delay Spread Statistics: The statistics of rms delay spread have been compiled from 1000 measured impulse responses. Fig. 16(a) shows the cumulative distributions of rms delay spread for the vacant tunnel. Curves (1) and (2) represent the cumulative distributions of 900-MHz channels for vertical and horizontal polarization, respectively. The maximum value of rms delay spread for vertical polarization is 8.68 ns and increases to 14.5 ns for the horizontal one. Curve (3) depicts the cumulative distribution of rms delay spread for 1800-MHz channel. A comparison between curves (1) with (3) shows a strong relation of the rms delay spread with frequency. Higher frequencies cause larger time-delay spread. The rms delay spreads are less than 3.01, 4.12, and 6.03 ns 50% of the time for 900-MHz vertically horizontally and 1800-MHz vertically polarized channels, respectively. The

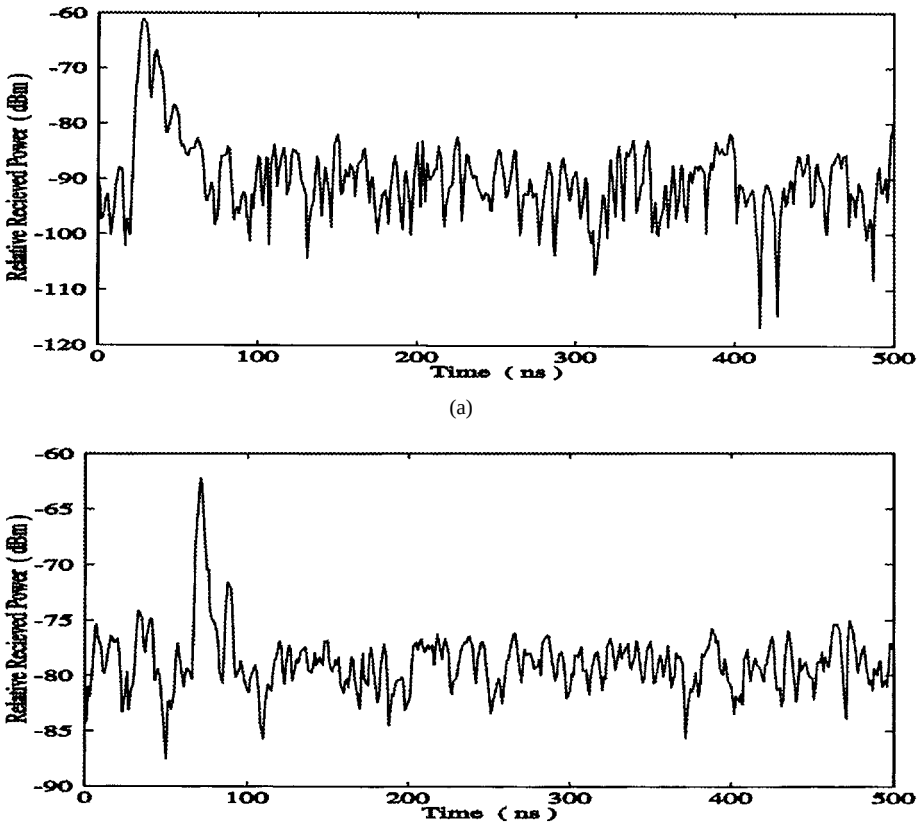

Fig. 14. (a) Vertically polarized impulse response measured at the frequency of 1800 MHz in the NS 173 tunnel for line-of-sight propagation path. (b) Vertically polarized impulse response measured at the frequency of 900 MHz with the transmitter outside and the receiver inside the NS 173 tunnel for line-of-sight propagation path.

maximum value of the rms delay spread for the 1800-MHz channel is 22 ns.

The cumulative distributions of rms delay spread obtained for the occupied tunnel are shown in Fig. 16(b). In general, rms delay spreads are larger than that of the vacant tunnel. The maximum rms delay spreads for 900-MHz vertically and horizontally polarized channels become 83.46 and 96.90 ns, respectively. The rms delay spreads are less than 21.7, 13, and 58.65 ns 50% of the time for 900-MHz vertically and horizontally and 1800-MHz vertically polarized channels, respectively. The dependence of rms delay spread on frequency still remains. The maximum rms delay spread for the 1800 vertically polarized channel is 103 ns.

It is well known that the ratio of rms delay spread to symbol duration in digital radio communication systems must be kept below 0.2 to have a tolerable intersymbol interference. Based on this criteria, the smaller rms delay spreads for the tunnel under vacant condition can support maximum data rates of 25, 13, and 9 Mb/s for 900-MHz vertically horizontally and 1800-MHz vertically polarized nonequalized channels, respectively. However, the maximum data rates would experience a sharp decrease to 2.4, 2.9, and 1.9 Mb/s for the tunnel under occupied condition.

V. Conclusion

The confined spaces of tunnels constitute considerably special radio propagation environments. This paper provides the propagation experimental data of both narrow and widebands at 900 and 1800 MHz based on measurements conducted in five tunnels.

Analysis of narrowband measurements revealed that power distance factors in the straight sections of the tunnels ranged from 1.87 to 4.49 with the standard deviation of 3.69–7.37, respectively. The propagation loss was insensitive to the location of the transmit antenna. Because of the dipole antenna used in the measurement, the antenna insertion loss was sensitive to the location.

The effects of pedestrians, vehicles, and curvature in tunnel environments on propagation were also investigated. The power distance factors for 900-MHz horizontally and vertically polarized signals were increased from 2.96 and 3.71 to 3.17 and 5.49 in an almost vacant to fully occupied underground market tunnel, respectively. Thus, pedestrians constituted an additional loss. The measurements in a coal-mine tunnel indicated that there was 13-dB shadowing loss at 900 MHz caused by the coal-mine train. The shadowing loss due to a car or truck was measured in a road tunnel with the truck causing a 6–10-dB additional loss and the car's shadowing effect being negligible. In comparison with either pedestrian or vehicle extra loss, the tunnel curvature yielded much more shadowing loss. Depending upon the location of the receive antenna, whether it was in the penumbra or deep shadow region, the shadowing losses were measured from 17 and 30 dB around the junction of the coal-mine tunnel at 900 MHz.

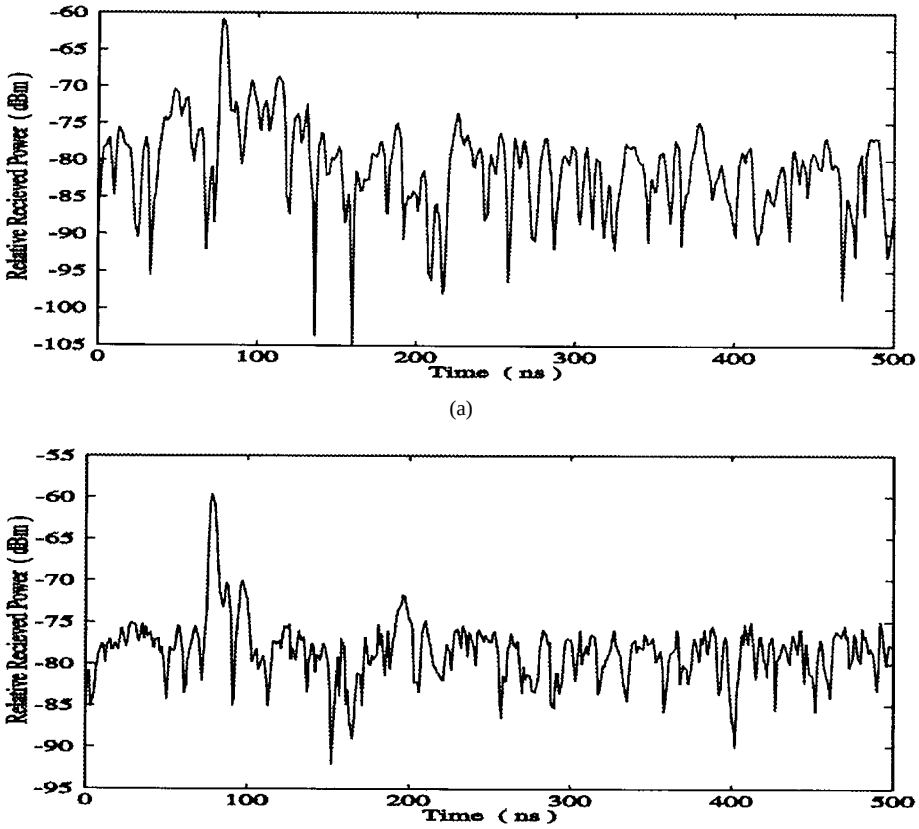

Fig. 15. (a) Horizontally polarized impulse response measured at the frequency of 900 MHz in the NS 173 tunnel for line-of-sight propagation blocked by a vehicle. (b) Horizontally polarized impulse response measured at the frequency of 900 MHz in the NS 173 tunnel occupied by a vehicle for line-of-sight propagation path.

The frequency dependence of shadowing loss on frequency was studied in the NS 173 tunnel. There was 9 dB more extra loss at 1800 MHz with respect to that of 900 MHz. This was due to a sharper penumbra region. It was also found that the shadowing loss was approximately the same for the horizontal and vertical polarization. This observation was consistent with the theory of geometrical optics.

The slow variations of the received signals in tunnel environments followed the lognormal distribution with averaged standard deviation of 4.7 dB for 900-MHz channels. The fast fading component distributions about the local median were obtained for all data files and compared to theoretical Rayleigh and Rician distributions. In the straight sections of the tunnel, fast fading of the received signal followed closely Rician distribution with $4 < K < 8$ dB. In the curved sections of the tunnel, it did not follow the Rayleigh distribution.

The tunnel wideband radio propagation channel was characterized in terms of rms delay spread and cumulative distributions. Analysis of wideband measurements indicated a broad coherent bandwidth characteristics of the channel. The rms delay spread showed a clear dependence on frequency. Higher frequency causes larger rms delay spread. The rms delay spread was found to be less than 25 and 103 ns for the vacant and occupied tunnel conditions, respectively. Thus, data rate up to 1 Mb/s without equalization can be supported in tunnel environments.

A new type of antenna that can match better to the tunnel environment to reduce the sensitivity of antenna insertion loss has been under study by the authors. The objectives are not only to improve the problem of antenna insertion loss, but also to minimize fading fluctuation and other factors from the system view point. The threshold depends on the tunnel environments and the existing hardware components. The impact of the change of the threshold on the conclusion of analysis has been pointed out by [11] and should be considered carefully in the deduction from the measured data.

APPENDIX

Five tunnels for different uses were selected to represent actual tunnel environments in our measurements. They are described as follows.

1) The TFH tunnel, reinforced with concrete, was built under the Fen River. The tunnel is rectangular with a width of 7.5 m, height of 4.0 m, and length of 2.0 km. The tunnel is open only at daytime for trucks, buses, and cars.
2) The TCMH tunnel complex consists of three main tunnels interconnected through several short branched tunnels. The tunnel complex was horizontally drilled in the western mountain. It has a slightly arch-shaped cross section and was reinforced with concrete. Measurements

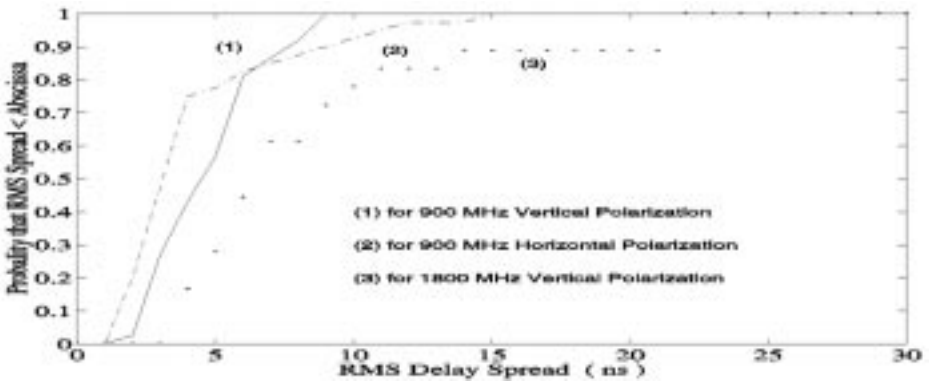

(a)

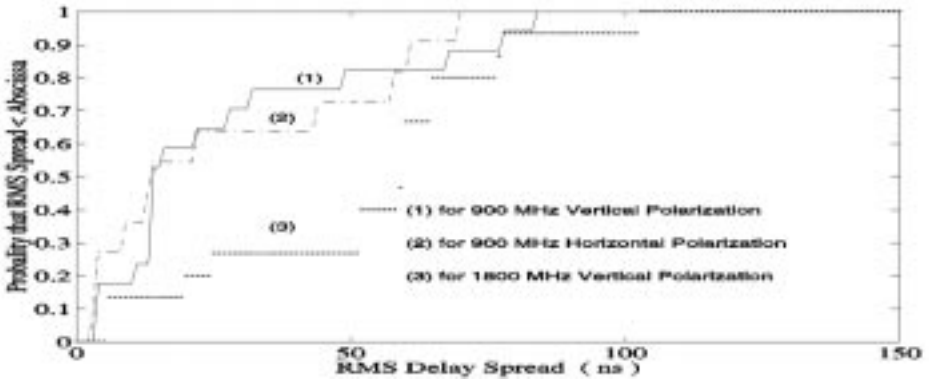

(b)

Fig. 16. (a) Probability that rms delay spread less than or equal to abscissa for the tunnel under empty condition. (b) Probability that rms delay spread less than or equal to abscissa for the tunnel under occupied condition.

were made in the vicinity of the junction between the central main tunnel and a branched one. The central main tunnel is approximately 10 km long, 3.0 m high, and 4.2 m wide, and the branched one is 140 m long, 3.0 m high, and 2.8 m wide. The explosion-proof lights are installed just beneath the tunnel roof at periodic intervals under which there are metallic tracks on the tunnel floor. The electricity lines for trains and other mining machinery are 0.8 m below the roof and are on the left-sided wall. The dc-powered trains are used to transport coal, materials, and miners. These moving trains are believed to have great effects on tunnel propagation, but the influences caused by those small fixed objects are usually negligible.

3) The SIMT tunnel is a small part of the underground labyrinth built in 1970's. The substratum of the tunnel is composed of loess and is reinforced with bricks. This rectangular tunnel of a 200-m length, 2-m height, and 2.4-m width can be roughly divided into three sections with the entry one of 100 m being the longest.
4) The TUM tunnel also has a slightly arch-shaped cross section and was reinforced with concrete. Entrances and exits in the Taiyuan Underground Market are situated at both ends through two inclined underpasses. The tunnel is straight with a width of 7.0 m, height of 3.7 m, and length of 120 m. Situated along the two side walls inside the tunnel are two rows of 0.4-m-wide and 2.0-m-high shelves occupied with various goods. In front of each row of shelves is a row of 0.8-m-wide and 1.0-m-high glass counters, between which is a narrow aisle for the market assistants. A 3.0-m-wide aisle is used as a passage for pedestrians and shoppers.
5) An NS 173 tunnel constructed of concrete is a subway with a rectangular cross section. The tunnel is 3.43 m wide, 2.6 m high, and 258.7 m long. It can be roughly divided into three sections. The middle section being 107.7 m long is straight while the two outer sections are slightly curved with the length of 51 and 100 m. The tunnel is often empty, with a few pedestrians occasionally passing by.

ACKNOWLEDGMENT

The authors wish to express their gratitude to Prof. G. Zheng, D. Poon, and T. Lo for their efforts in the measurements. The authors would also like to thank Prof. J. H. Sheng for his support and encouragement.

REFERENCES

[1] J. D. Parsons, *The Mobile Radio Propagation Channel.* London, U.K.: Pentech, 1992.
[2] H. H. Xia, H. L. Bertoni, L. R. Maciel, A. L. Stewart, and R. Rowe, "Radio propagation characteristics for line-of-sight microcellular and personal communications," *IEEE Trans. Antennas Propagat.*, vol. 41, no. 10, pp. 1439–1447, 1993.
[3] S. Mockford, "Narrowband characterization of UHF mobile radio channels in rural areas," Ph.D. dissertation, University of Liverpool, U.K., 1989.
[4] R. J. Van, "Measurements of the wideband radio channel characteristics for rural, residential, and suburban areas," *IEEE Trans. Veh. Technol.*, vol. 36, no. 1, pp. 2–6, 1987.

[5] D. C. Cox, "Delay-Doppler characteristics of multipath propagation at 910 MHz in a suburban mobile radio environment," *IEEE Trans. Antennas Propagat.*, vol. 20, no. 9, pp. 625–635, 1972.
[6] A. S. Bajwa and J. D. Parsons, "Small area characterization of UHF urban and suburban mobile radio propagation," *Proc. Inst. Elect. Eng.*, vol. 129, pt. F, no. 2, pp. 102–109, 1982.
[7] A. J. Rustako, G. J. Owens, and R. S. Roman, "Radio propagation at microwave frequencies for line-of-sight microcellular mobile and personal communications," *IEEE Trans. Veh. Technol.*, vol. 40, no. 2, pp. 203–210, 1991.
[8] R. J. C. Bultitude and G. K. Bedal, "Propagation characteristics on microcellular urban mobile radio channels at 910 MHz," *IEEE J. Select. Areas Commun.*, vol. 7, no. 1, pp. 31–39, 1989.
[9] H. Hashemi, "Simulation of the urban radio propagation channel," *IEEE Trans. Veh. Technol.*, vol. 28, no. 3, pp. 213–225, 1979.
[10] D. C. Cox, "Multipath delay spread and path loss correlation for 910 MHz urban mobile radio propagation," *IEEE Trans. Veh. Technol.*, vol. 26, no. 2, pp. 340–344, 1977.
[11] T. S. Rappaport, S. Y. Seidel, and R. Singh, "900-MHz multipath propagation measurements for U.S. digital cellular radiotelephone," *IEEE Trans. Veh. Technol.*, vol. 39, no. 2, pp. 132–139, 1990.
[12] N. Amitay, L. J. Greenstein, and G. J. Owens, "Measurements-based estimates of bit-error-rate performance in urban LOS microcells at 900 MHz," *IEEE Trans. Veh. Technol.*, vol. 41, no. 4, pp. 414–423, 1992.
[13] A. J. Goldsmith and L. J. Greenstein, "A measurement-based model for predicting coverage areas of urban microcells," *IEEE J. Select. Areas Commun.*, vol. 11, no. 7, pp. 1013–1023, 1993.
[14] J. H. Whitteker, "Measurements of path loss at 910 MHz for proposed microcell urban mobile systems," *IEEE Trans. Veh. Technol.*, vol. 37, no. 3, pp. 125–129, 1988.
[15] S. T. S. Chia, R. Steele, E. Green, and A. Baran, "Propagation and bit error ratio measurements for a microcellular system," *J. IERE*, vol. 57, no. 6, pp. S255–S266, 1987.
[16] W. Honcharenko, H. L. Bertoni, J. L. Dailing, J. Qian, and H. D. Ye, "Mechanisms governing UHF propagation on single floors in modern office buildings," *IEEE Trans. Veh. Technol.*, vol. 41, no. 4, pp. 496–504, 1992.
[17] W. Honcharenko, H. L. Bertoni, and J. L. Dailing, "Mechanisms governing propagation between different floors in buildings," *IEEE Trans. Antennas Propagat.*, vol. 41, no. 6, pp. 787–790, 1993.
[18] S. Y. Seidel and T. S. Rappaport, "914 MHz path loss prediction models for wireless communications in multifloored buildings," *IEEE Trans. Antennas Propagat.*, vol. 40, no. 2, pp. 207–217, 1992.
[19] D. M. J. Devasirvatham, "Time delay spread and signal level measurements of 850 MHz radio waves in building environments," *IEEE Trans. Antennas Propagat.*, vol. 34, no. 11, pp. 1300–1305, 1986.
[20] D. M. J. Devasirvatham, "A comparison of time delay spread and signal level measurements within two dissimilar office buildings," *IEEE Trans. Antennas Propagat.*, vol. 35, no. 3, pp. 319–324, 1987.
[21] H. Hashemi and D. Tholl, "Statistical modeling and simulation of the RMS delay spread of indoor radio propagation channels," *IEEE Trans. Veh. Technol.*, vol. 43, no. 1, pp. 110–119, 1994.
[22] A. A. M. Saleh and R. A. Valenzuela, "A statistical model for indoor multipath propagation," *IEEE J. Select. Areas Commun.*, vol. 5, no. 2, pp. 128–137, 1987.
[23] S. J. Howard and K. Pahlavan, "Autoregressive modeling of wideband indoor radio propagation," *IEEE Trans. Commun.*, vol. 40, no. 9, pp. 1540–1552, 1992.
[24] R. J. C. Bultitude, S. A. Mahmoud, and W. A. Sullivan, "A comparison of indoor radio propagation characteristics at 910 MHz and 1.75 GHz," *IEEE J. Select. Areas Commun.*, vol. 7, no. 1, pp. 20–30, 1989.
[25] T. S. Rappaport and C. D. Mcgillem, "UHF fading in factories," *IEEE J. Select. Areas Commun.*, vol. 7, no. 1, pp. 40–48, 1989.
[26] T. S. Rappaport, "Indoor radio communications for factories of the future," *IEEE Commun. Mag.*, pp. 15–24, May 1989.
[27] T. S. Rappaport, "Characterization of UHF multipath radio channels in factory buildings," *IEEE Trans. Antennas Propagat.*, vol. 37, no. 8, pp. 1058–1069, 1989.
[28] A. G. Emslie, R. L. Lagace, and P. F. Strong, "Theory of the propagation of UHF radio waves in coal mine tunnels," *IEEE Trans. Antennas Propagat.*, vol. 23, no. 2, pp. 192–205, 1975.
[29] S. F. Mahmoud and J. R. Wait, "Geometrical optical approach for electromagnetic wave propagation in rectangular mine tunnels," *Radio Sci.*, vol. 9, no. 12, pp. 1147–1158, 1974.
[30] L. Deryck, "Natural propagation of electromagnetic waves in tunnels," *IEEE Trans. Veh. Technol.*, vol. 27, no. 3, pp. 145–150, 1978.
[31] J. Chiba, T. Inaba, Y. Kuwamoto, O. Banno, and R. Sato, "Radio communication in tunnels," *IEEE Trans. Microwave Theory Tech.*, vol. 26, no. 6, pp. 439–443, 1978.
[32] P. Delogne, "EM propagation in tunnels," *IEEE Trans. Antennas Propagat.*, vol. 39, no. 3, pp. 401–405, 1991.
[33] Ph. Mariage, M. Lienard, and P. Degauque, "Theoretical and experimental approach of the propagation of high frequency waves in road tunnels," *IEEE Trans. Antennas Propagat.*, vol. 42, no. 1, pp. 75–81, 1994.
[34] Y. Yamaguchi, T. Abe, T. Sekiguchi, and J. Chiba, "Attenuation constants of UHF radio waves in arched tunnels," *IEEE Trans. Microwave Theory Tech.*, vol. 33, no. 8, pp. 714–718, 1985.
[35] W. C. Jakes, *Microwave Mobile Communications*. New York: Wiley, 1974.
[36] S. O. Rice, "Mathematical analysis of random noise," *Bell Syst. Tech. J.*, vol. 23, no. 7, pp. 282–332, 1944.
[37] A. Papoulis, *Probability, Random Variables, and Stochastic Processes*. New York: McGraw-Hill, 1965, pp. 498–499.

Y. P. Zhang received the B.Eng. and M.Eng. degrees in electronic engineering from Taiyuan University of Science and Technology, Taiyuan, Shanxi, PRC, in 1982 and 1987 and the Ph.D. degree in electronic engineering from the Chinese University of Hong Kong, Hong Kong, in 1995.

In China, he worked at Shanxi Electronic Industry Bureau, Shanxi Institute of Mining and Technology, and Taiyuan University of Science and Technology intermittently from 1982 to 1996. In Britain, he studied new-generation digital mobile and personal communications from 1990 to 1992. In Hong Kong, he studied at the Chinese University from February 1993 to December 1995 and was one of the 1995 CU Outstanding Graduates. He is currently working at the City University of Hong Kong. He has been working on mobile communications, radio channel characterization, radio-frequency circuit design and engineering, small and smart antennas, earth-penetrating radar, and subsurface microcellular and personal digital communications systems and networks.

Dr. Zhang received the Technical Cooperation Award in 1990 from the Chinese and British Governments for his contribution to the advancement of subsurface radio communications. He received the ORS Award in 1992 from the British Government for his academic excellence at the University of Liverpool.

Y. Hwang received the B.S. degree from National Taiwan University, Taipei, Taiwan, in 1963, the M.S. degree from the Institute of Electronics of National Chiao-Tung University, Hsin Chu, Taiwan, in 1965, the Ph.D. degree from Ohio State University, Columbus, in 1973, and the MBA degree from the Golden Gate University, San Francisco, CA, in 1982.

He worked in the ElectroScience Laboratory of the Ohio State University in 1974 for one year. In 1975, he was with the Department of Antenna Engineering of Ford Aerospace, where he was a Section Supervisor in the Advanced Antenna Technology Section. He left Aerospace in 1992. From 1993 to 1995, he was in the Department of Electronic Engineering, Chinese University of Hong Kong. He is currently in the Department of Electronic Engineering, City University of Hong Kong. He has been working on the geometrical theory of diffraction, satellite antennas, and ground antennas. He has developed a multibeam antenna system, a frequency-selective surface for multifrequency bands reflector antenna system and high-power operation, a wideband dual-circularly polarized microstrip phased-array antenna, and an S-band MMIC phased-array antenna. Recently, he has developed a high-radiation-efficiency printed antenna with very high permittivity materials and transmit phased array without a beamforming network and is studying EM wave-propagation characteristics in confined space.

Dr. Hwang received the 1989 Space Systems Division Outstanding Research Award and the 1990 Exceptional Inventiveness Award from Ford Aerospace Space Division.